# Collective Hydrogen-Bond Dynamics Dictates the Electronic Structure of Aqueous I$_3^-$

Ida Josefsson,[a] Susanna K. Eriksson,[b] Niklas Ottosson,[c] Gunnar Öhrwall,[d] Hans Siegbahn,[e] Anders Hagfeldt,[b] Håkan Rensmo,[e] Olle Björneholm,[e] and Michael Odelius*[a]

The molecular and electronic structures of aqueous I$_3^-$ and I$^-$ ions have been investigated through ab initio molecular dynamics (MD) simulations and photoelectron (PE) spectroscopy of the iodine 4d core levels. Against the background of the theoretical simulations, data from our I4d PE measurements is shown to contain evidence of coupled solute-solvent dynamics. The MD simulations reveal large amplitude fluctuations in the I–I distances, which couple to the collective rearrangement of the hydrogen bonding network around the I$_3^-$ ion. Due to the high polarizability in the I$_3^-$ ion, the asymmetric I–I vibration reaches partially dissociated configurations, for which the electronic structure resembles that of I$_2$ + I$^-$. The charge localization in the I$_3^-$ ion is found to be moderated by hydrogen-bonding. As seen in the PE spectrum, these soft molecular vibrations are important for the electronic properties of the I$_3^-$ ion in solution and may play an important role in its electrochemical function.

## 1 Introduction

Understanding the fundamental physical chemistry of the I$^-$/I$_3^-$ redox couple is of great interest for energy research, especially owing to its use in dye-sensitized solar cells (DSSCs)[1–9], which have gradually turned into a competitive technology for harvesting solar energy. Already in early DSSC designs, I$^-$/I$_3^-$ was used as an agent for regenerating the photooxidized dye. Alternatives are currently being investigated with special focus on optimizing the performance of cobalt complexes as hole conductor[8,10] as well as perovskites[11,12]. However, the original I$^-$/I$_3^-$ redox couple is still competitive in terms of performance and it has been used in many different electrolyte compositions, often with acetonitrile as solvent. Aqueous solutions are of particular interest in applied systems for environmental and cost reasons and since there are problems associated with creating a durable sealing of the solar cells, resulting in water impurities after long-time usage[7,13–16]. To guide the development of electrochemical systems such as DSSCs, it is desirable to obtain detailed microscopic information about the chemistry of the redox couple, and in the present study, the solvation of I$_3^-$ in aqueous solution is investigated at an atomic level. Vibrational Raman measurements of the I$_3^-$ ion have shown that the asymmetric stretch is activated in protic solvents, like ethanol[17]. Extended X-ray absorption fine structure (EXAFS) measurements[18,19] have given direct information on the geometry of the I$_3^-$ ion in different solvents, confirming the soft nature of the I$_3^-$ ion in protic solvents. MD simulations, employing a semi-empirical valence bond model[20–22], explain the experimental results in terms of a symmetry breaking of the ion, induced by strong solvent interactions. This effect is particularly strong in water.

In this study, ab initio MD simulations and I4d core-level spectroscopy, which are complementary sources of information on the electronic structure, are used to investigate the solvation of the I$_3^-$ ion. X-ray photoelectron spectroscopy is an element specific probe of electronic core levels and has proven to be a valuable source of information of the electronic structure in solution[23–26]. In combination with ab initio molecular dynamics(MD) simulations, we can in great detail investigate the solvation of the individual iodine atoms in I$_3^-$(aq). The measured core-level I4d spectra are compared to simulated spectra using high-level quantum chemistry, through which we can relate the core-level shifts to the geometric and electronic structure of aqueous I$_3^-$. Both PE experiments and MD simulations are performed on LiI$_3$ and LiI solutions, to investigate the structure and dynamics in the hydration shells around the ions. Quantum chemistry, used to compute PE spectra along the MD trajectory, provides insights with molecular resolution for the interpretation of the PE spectrum of aqueous LiI$_3$.

a *Department of Physics, Stockholm University, AlbaNova University Center, 106 91 Stockholm, Sweden*
b *Department of Chemistry- Ångström, Uppsala University, Box 523, 751 20 Uppsala, Sweden*
c *FOM institute AMOLF, Science Park 102, 1098 XG Amsterdam*
d *MAX IV Laboratory, Lund University, Box 118, 221 00 Lund, Sweden*
e *Department of Physics and Astronomy, Uppsala University, Box 530, 752 21 Uppsala, Sweden*
* *. Fax: +46 8 5537 8601; Tel: +46 8 5537 8713; E-mail: odelius@fysik.su.se*

## 2 Experimental

X-ray photoelectron spectroscopy measurements were performed using synchrotron radiation at the undulator beamlines I411 at the Swedish national laboratory MAX IV in Lund (photon energy 100 eV) and at U41-PGM at the synchrotron facility BESSY II at HZB in Berlin (photon energies 200 and 600 eV). The proportions of LiI and $I_2$ were selected to determine the $I_3^-$ concentration in the solution samples. In water and acetonitrile, we prepared both 0.5 molar (M) LiI solutions and mixtures of 0.25 M $I^-$ and 0.25 M $I_3^-$ (obtained by mixing LiI and $I_2$ in a ratio of 2:1). An ethanol solution containing 0.5 M $I_3^-$ was obtained by mixing LiI and $I_2$ in a ratio of 1:1. The solutions were prepared just before each experiment, mixing chemicals (purchased from Sigma-Aldrich with purity > 99%) with highly demineralized water, ethanol (99.5 %) or acetonitrile (anhydrous 99.8 %). The liquid samples were injected into the evacuated experimental chamber ($\sim 10^{-5}$ mbar) as a liquid micro-jet with a diameter of approximately 20 $\mu$m, by means of backing pressure from a HPLC pump. The temperature of the samples was estimated to be 5$\pm$5 °C. The experiment and the setups are described in detail elsewhere.[23,27] The peak fits were performed by using a Voigt profile line with spin–orbit splitting set to 1.7 eV and a intensity ratio for the $I4d_{3/2}$ and $I4d_{5/2}$ contributions set to 0.75 obtained from experiments of solutions with pure LiI. The pure gas phase $I_2$-signal was obtained by lowering the liquid-jet just below the X-ray beam.

## 3 Computational

Ab initio (Car-Parrinello) MD simulations were performed with the CPMD code[28,29] of a pair of ions, solvated in 100 water molecules in cubic simulation cells with periodic boundary conditions and cell sides of 15.0328 Å for $LiI_3$(aq) and 14.6791 Å for LiI(aq), respectively. To obtain reasonable input values for the ab initio simulation, the densities and initial conditions were obtained from classical MD simulations, which will be described in a forthcoming publication[30]. Each ab initio MD simulation was equilibrated for a few picoseconds and then sampled for 40 ps. The systems were deuterated, and in the Car-Parrinello algorithm[28], a fictitious energy mass of 800 a.u. was combined with a time-step of 6 a.u. The electronic structure was described with density functional theory (DFT) with a gradient corrected functional (BLYP) augmented with van der Waals interactions[31–33]. The Kohn-Sham wave-functions were expressed in a plane wave expansion with a 70 Ry kinetic energy cut-off. For oxygen a Troullier-Martins pseudo-potential[34] expressed in the Kleinman-Bylander form[35] was used. Hydrogen was represented by a local pseudo-potential, parametrized with one Gaussian. Goedecker pseudo-potentials[36,37] were used for the ions.

In order to make direct contact with the PE experiments, spectral calculations were performed from structures obtained in the MD simulations. Theoretical PE spectra of $I_3^-$(aq) were sampled over 10 configurations, evenly distributed over the full simulation trajectory of $LiI_3$(aq). Explicit solvent effects were determined through cluster calculations with and without the surrounding solvent, including all water molecules with the oxygen within a 4.8 Å radius from any iodine atom (20–30 molecules). Theoretical I4d PE spectra of $I_3^-$(aq) and $I_3^-$(g) were computed by an explicit description of the initial singlet ground state and final doublet states in a vertical core-ionization process. The discrete energy levels were broadened with a Gaussian function of 1.1 eV full width at half maximum (FWHM) to allow for direct comparison with experiment. The PE simulations were based on relativistic complete active space self-consistent field (CASSCF) calculations[38] using the MOLCAS-7 software[39]. Scalar relativistic effects were introduced via the second order Douglas-Kroll-Hess Hamiltonian[40,41] in conjunction with a relativistic all-electron ANO-RCC basis set, contracted to VTZP quality[42]. Spin–orbit coupling effects, essential to reproduce the $I4d_{3/2}$ and $I4d_{5/2}$ splitting, were computed using the state-interaction technique[43]. In order to allow for ionization of the iodine 4d core-levels, the active space was chosen to contain all 4d orbitals while the rest of the occupied orbitals were left inactive. To ensure convergence in the CASSCF calculations, orbital rotations were not allowed between the 4d subspace and the remaining occupied orbitals, but in a freeze/thaw procedure the orbital spaces communicate through the unoccupied orbitals. For the final states, the orbitals were optimized for the energy average of all core-ionized states with equal weights. Suitable starting orbitals for the CASSCF procedure were generated in a single-configuration SCF calculation, with each 4d orbital carrying an equal fraction of the core hole. The charge localization in the electronic structure of the $I_3^-$ under various degree of geometrical distortion was analyzed in the CASSCF calculations in MOLCAS-7, using the LoProp scheme[44], and in CPMD, Löwdin charges were determined using a projection of the wavefunction onto a local Slater orbital basis set. In the latter, the charge decomposition is highly sensitive to the choice of basis set. In order to obtain reasonable net charge of the $I_3^-$ ion, the Slater basis set on iodine was altered to a 5spd ($\alpha$=2.4 au.) and augmented with 6sp ($\alpha$=1.6 au.). However, the trend in the sampling of charges is independent of the choice of basis set.

## 4 Results

In Figure 1, the MD simulation results for the internal geometry of the $I_3^-$(aq) ion are presented. The simulation
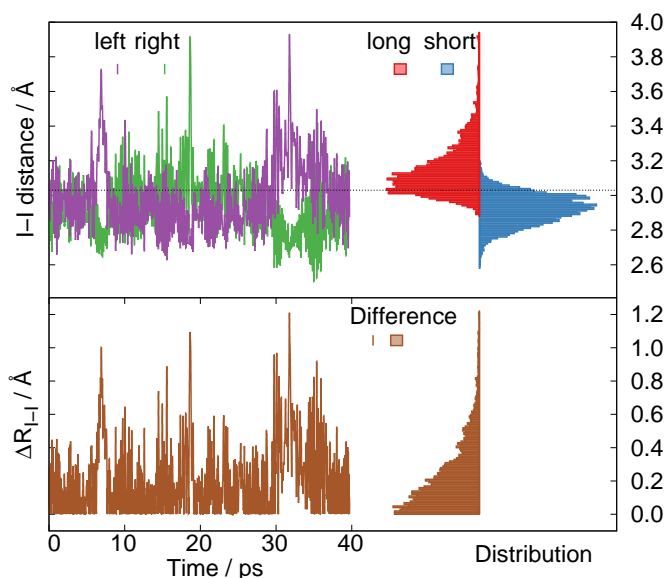
**Fig. 1** During the molecular dynamics simulation of LiI$_3$(aq), the time evolution in the I–I bond lengths contains periods of a pronounced asymmetry, which is highlighted by sampling of the longest and shortest I–I bond. We also display the bond length difference which is identified as the key measure for the electronic properties of the I$_3^-$ (aq) ion.

data, with the I–I bonds characterized by involving either the "left" or "right" terminal atom, shows large amplitude bond length fluctuations in the I$_3^-$ ion. In the time trace in Figure 1, both I–I distances repeatedly attains values in the asymmetric I–I vibration exceeding that of a covalent bond. Even very distorted configurations constitute a significant part of the total geometry distribution of I$_3^-$(aq): As seen from the respective distributions of the longest and shortest I–I separation at each time-step in Figure 1, the I$_3^-$ molecule reached partially dissociated configurations extending to almost 4 Å separation. The average I–I bond length in the MD simulation (3.03±0.16 Å) agrees with the optimized bond length of the symmetric molecule (3.02 Å (CPMD/BLYP) and 3.00 Å (MOLCAS/CASSCF)). Our sampled results on the structure of the I$_3^-$ ion (I$-$I$_{long}$=3.14 Å, I$-$I$_{short}$=2.92 Å, I$-$I$_{diff}$=0.22 Å, I$-$I$_{sum}$=6.07 Å and an I$-$I$-$I angle of 170°) are in qualitative agreement with recent EXAFS measurements [18] (I$-$I$_{long}$=3.38±0.03 Å, I$-$I$_{short}$=2.93±0.03 Å, I$-$I$_{diff}$=0.45±0.04 Å, I$-$I$_{sum}$=6.13±0.14 Å and an I$-$I$-$I angle of 153°). For a more detailed comparison one would need to calculate the EXAFS signal from configurations sampled over the MD trajectory including multiple-scattering. We can also notice that in the CPMD simulation, the angular distortion is not correlated with the bond distance asymmetry.

To rationalize the fluctuations in the internal geometry, we consider the inter-molecular interactions. In Figure 2, the hy-
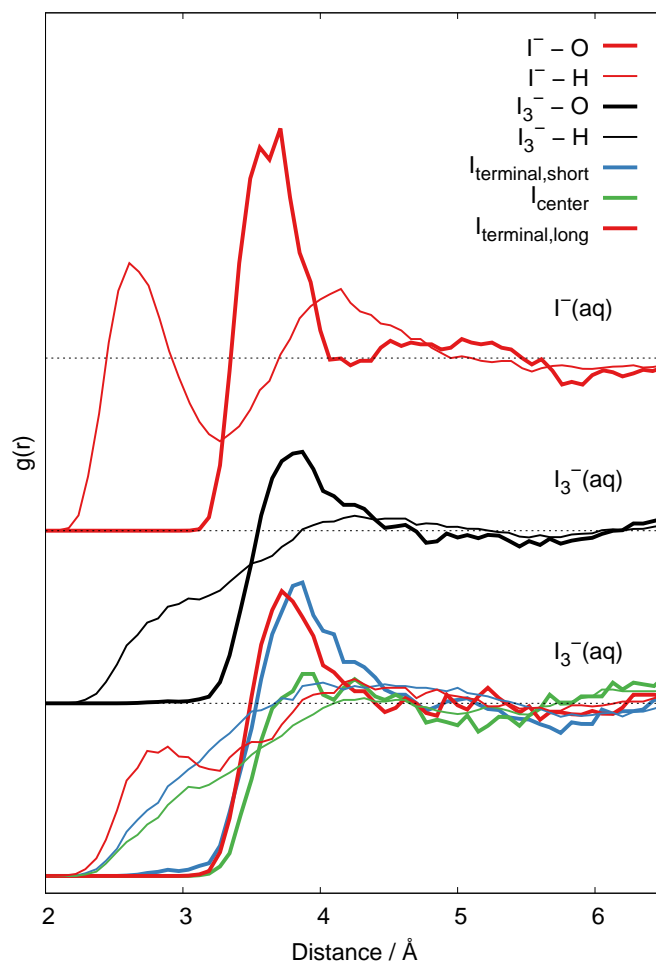


**Fig. 2** The I–O (thick lines) and I–H (thin lines) radial distribution functions for the hydration of the I$_3^-$ and I$^-$ ions, analyzed by partitioning the contributions from the terminal and center atoms in the I$_3^-$ ion, indicate similar solvation of I$^-$ and of the I$_3^-$ terminal atom at the largest I–I separation.

dration structures of the I$_3^-$ ion in LiI$_3$(aq) and the I$^-$ ion in LiI(aq) are analyzed in terms of iodine-oxygen and iodine-hydrogen radial distribution functions (RDFs). The I-O RDF shows a distinct first solvation shell around the I$^-$ ion with 8.4±0.9 water molecules surrounding the ion when the shell radius is taken to be the first minimum at 4.22 Å. There is a clear signature of H-bonding in the I-H RDF, from which we derived that there are 6.1±0.3 H-bonds to the I$^-$ ion. This is in close agreement with the results obtained in earlier ab initio MD simulations [45]. The I$_3^-$ ion has overall a much less pronounced H-bonding, but the partitioning of the total I-O and I-H RDFs into contributions from the different terminal and center atoms provides more information about the hydrogen bonding pattern around the ion. The I-H RDFs in Figure 2 show that solvation of the I atom which is located at

the longest distance to its neighbor in $I_3^-$ resembles that of aqueous $I^-$. A similar asymmetry in solvation of the terminal iodine atoms for a distorted $I_3^-$ has been noticed in previous theoretical simulations [46]. During the MD simulation of $LiI_3(aq)$, the probability of finding a hydrogen atom at the typical H-bond distance from the terminal iodine in the long bond ($I_{terminal,long}$) is enhanced, whereas the terminal iodine in the short bond ($I_{terminal,short}$) and the central iodine atom ($I_{center}$) do not show the same tendency to accept hydrogen bonds. We can hence conclude that there is a strong coupling between the I–I distance fluctuations and a collective hydrogen bond rearrangement in the surrounding water network. Through interactions with water, the $I_3^-$ ion is distorted along the asymmetric I–I stretch mode. Notice that the I-O RDFs of the terminal iodine atoms only differ in a slight swelling of the first hydration shell, which indicates that the process responsible for changes in hydration involves reorientations of the water molecules. To confirm that the large amplitude fluctuations in the highly polarizable tri-iodide ion were not an artifact of the Car-Parrinello algorithm, a comparison to Born-Oppenheimer (BO) dynamics (in which the wave-function is converged at each time-step) was made for the last 3 ps. The BOMD simulation exhibited distance fluctuations of comparable magnitude.
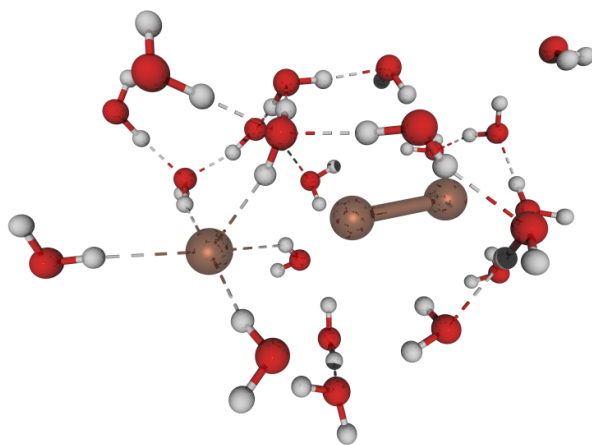


**Fig. 3** The solvation of $I_3^-$(aq) in the molecular dynamics simulation reveals that the asymmetric I–I stretch of $I_3^-$ is associated with a pronounced hydrogen bonding around the terminal iodide atom in the elongated bond.

Thus, by distinguishing between the terminal iodine atoms involved in short and long I–I bond distances, in the sampling of the RDFs, we gain insight into the solvation $I_3^-$(aq). As the representative simulation snapshot in Figure 3 clearly illustrates, the (almost) detached iodine atom is well solvated by H-bonding, whereas the remaining $I_2$ moiety is only weakly solvated.

The solvent-induced fluctuations in the asymmetric I–I stretch are associated with a large change in electronic structure. The population analysis of the 10 CASSCF calculations of geometries sampled from the CPMD simulation suggests that geometrical symmetry breaking of the $I_3^-$ ion mainly causes a charge redistribution between the terminal atom centers. Hence, we performed more extensive sampling and in Figure 4, we plot the Löwdin charge distribution from DFT calculations in CPMD within the $I_3^-$ ion as a function of the distortion parameter $\Delta R_{I-I}$ (compare Figure 1). The sampling confirms that the central charge is essentially independent of distortion as the charge localizes on the terminal iodine atom in the long bond. Notably, there is a near linear relationship in charge redistribution between the terminal sites as a function of difference in bond distance. The charge localization thus correlate with the asymmetry in hydrogen bonding.
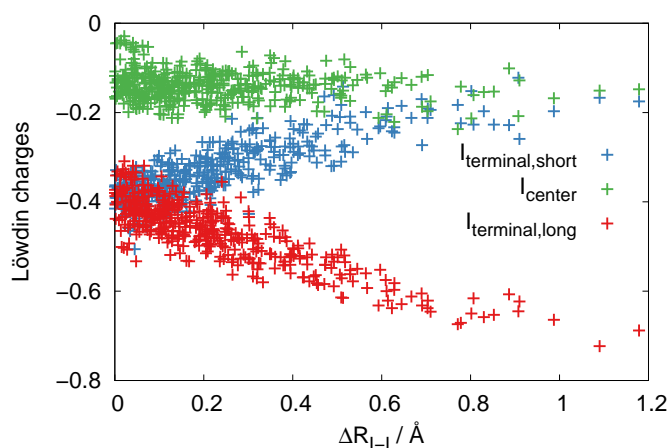


**Fig. 4** Partial Löwdin charges on the different atomic sites of the aqueous $I_3^-$ ion as a function of bond distance asymmetry, obtained from sampling 1000 configurations during the molecular dynamics simulation of $LiI_3(aq)$.

To test the validity of the MD simulations we now turn to simulations of I4d core-level PE spectra, in which the electronic structure can be experimentally monitored. In Figure 5, the calculated I4d PE spectra of the naked $I_3^-$ ion, sampled over the CPMD simulation, show a clear trend when ordered according to the I–I distance asymmetry: When the molecule is distorted, the doublet corresponding to photoemission from the terminal atom involved in the elongated bond gradually shifts to lower binding energy, while the binding energy of the other terminal atom increases. The binding energy shifts are correlated with the charge density on the respective core-ionized atom and, as Figure 4 illustrates, elongation of an I–I bond is associated with electron density transferred from the iodine terminal atom in the short I–I bond to that in the long I–I bond. Accordingly, the 4d electrons localized at $I_{terminal,long}$
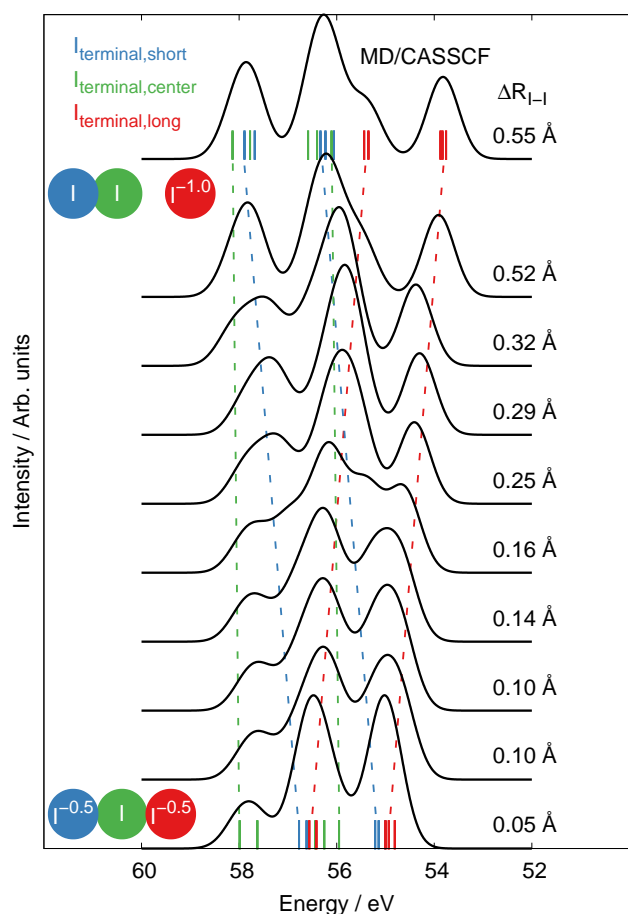
**Fig. 5** Calculated I4d core-level photoelectron (PE) spectra of the naked $I_3^-$ ion, sampled over configurations from the molecular dynamics (MD) simulation of $LiI_3$(aq) and ordered according to increasing bond asymmetry. For the most symmetric and asymmetric configurations, the discrete transitions are included with the same coloring scheme as in Figure 4 showing the contribution from each iodine atom to the photoelectron spectrum.



**Fig. 6** Experimental PE spectra in solutions of water ($H_2O$), acetonitrile (AcCN) and ethanol (EtOH). The decomposition of the experimental PE spectrum of $I_3^-$ from ethanol solution is presented.

become less strongly bound, since it has negative charge and therefore the binding energy will decrease while the decreased negative charge (approaching neutral) on the opposite terminal atom leads to higher binding energy – its contribution to the PE spectrum thus approaching the central iodine peak. Since the charge on the central iodine atom does not depend on the geometric fluctuations, the central peak position is essentially fixed in the calculated spectra. In summary, the charge distribution within $I_3^-$ directly determines the shape of the I4d PE spectrum and as a consequence of a geometry distortion, the doublet peak originating from photoemission from the terminal atoms separate into two sets of peaks.

We now turn to the experimental I4d PE spectra of $I_3^-$, presented in Figure 6. To provide a reference to the aqueous sam-

ples of primary interest, data for less hydrogen donating solvents, ethanol and acetonitrile, are also shown. Deconvoluted spectra representing $I_3^-$ in Figure 6 are presented from bottom to top: In ethanol (EtOH), the solution contained only $Li^+$ and $I_3^-$ and no further analysis was needed to extract the relevant spectrum. In acetonitrile (AcCN), the $I_3^-$ contribution was obtained by subtracting a spectrum from a pure LiI solution. Similar to the ethanol solution, the $I_3^-$ spectrum in acetonitrile can be deconvoluted into contributions from the terminal and center parts[30]. The aqueous $I_3^-$(aq) spectrum shown in the top trace in Figure 6 is obtained through subtraction of experimental spectra of both LiI and $I_2$(g) from the total spectrum. The weight of the subtracted $I_2$ contribution was chosen to entirely remove the gas line whereas the intensity of the $I^-$ contributions were chosen to approximately 1/3 of the total intensity which is the stochiometric relationship with any surface effects disregarded. In contrast to the other solvents, peak fitting

of aqueous solution is complicated and the resulting curve is not possible to deconvolute assuming a linear and symmetric $I_3^-$.
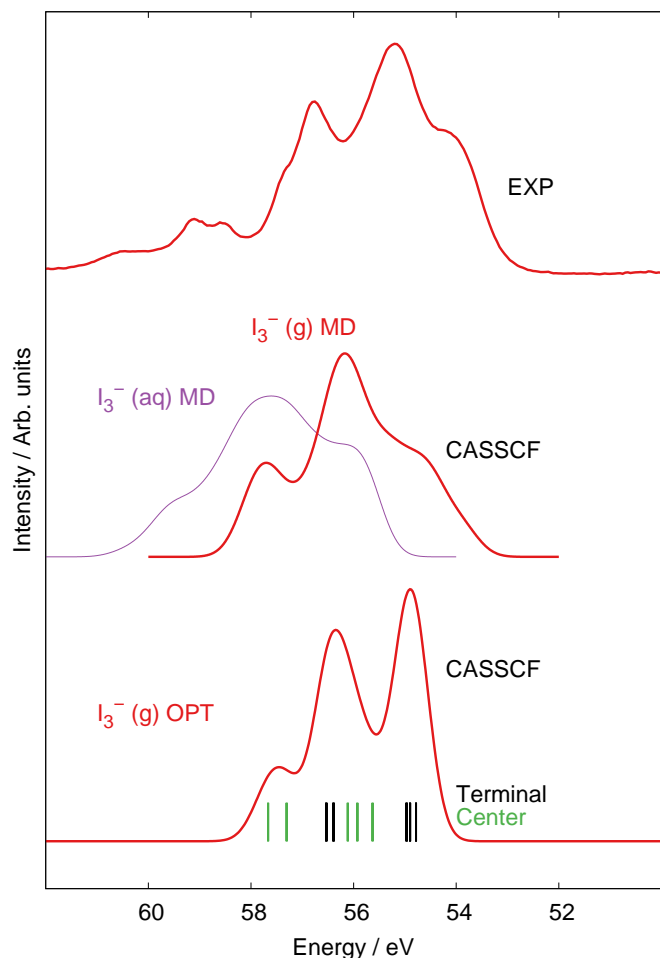


**Fig. 7** Bottom: The calculated spectrum of optimized $I_3^-$ (g), including the discrete binding energies assigned to the terminal and center iodine positions. Middle: I4d PE spectra averaged over the MD sampling, with and without solvation. Top: The net experimental spectra of $I_3^-$ (aq) from Figure 6.

The averages of the individual calculated spectra of naked and hydrated $I_3^-$, respectively, are presented in Figure 7. In comparison and contrast to the sampled spectrum in water including asymmetric distortions, we show that the calculated spectrum of the optimized symmetric $I_3^-$ ion in Figure 7 and the experimental PE spectrum of $I_3^-$ from ethanol solution in Figure 6 are similar in shape and can be decomposed into contributions from the terminal and center iodine positions. However, the calculated spectra needs to be shifted by -1.5 eV to quantitatively agree with experiments. This is primarily due to the lack of dynamic electron correlation in the theoretical description[30]. The most pronounced feature when averaging

over distorted geometries from the MD simulation is a broadening in the low binding energy direction. Addition of the first hydration shell in the cluster calculations shifts each spectrum about 1.5 eV to higher binding energy. The average PE spectra are qualitatively similar, but the presence of the surrounding solvent gives a considerable broadening of the lines. The variation in the solvation shifts is overestimated due to the finite cluster size and therefore the resulting average in Figure 7 is broadened too much by the solvent interactions.

The experimental PE spectrum of aqueous $I_3^-$ resembles that obtained from the sampling over the MD simulation of $LiI_3$(aq), showing a marked broadening of the spectrum in the low binding energy direction. According to the theoretical analysis, the low-binding energy shoulder (only present in aqueous solution) is the signature of geometric and electronic asymmetry in the $I_3^-$ ion. As a complication, the experimental spectra contain different contributions from $Li^+$, $I^-$, and $I_2$ species, due to the solvent dependence in the equilibrium constant for $I_3^- \rightleftharpoons I^- + I_2$ (strongly pushed towards left in organic solvents), leading to subsequent evaporation of $I_2$ in aqueous solution. The concentration of $I_2$ in the aqueous solution is in the order of 0.001 M and the intensity in the PE spectrum of dissolved $I_2$ is therefore still negligible. The $Li^+$ contribution appears in the spectra at a binding energy slightly above 60 eV while the spin–orbit split doublets of $I_2$ and $I^-$ have a $I4d_{5/2}$ peak at about 57.5 eV and 53.5 eV respectively.

Our interpretation of the PE spectra relies on the robustness of the subtraction scheme used to extract the $I_3^-$ contribution and we elaborate on this point in Figure 8. In panel a in Figure 8, we show that independent experiments (higher photon energy) with the more focused X-ray beam at BESSY II confirm that the $I_2$ signal is essentially removed in the presented $I_3^-$ spectra in Figure 6. The remaining difference, indicates that we might also have a $I_2$ signal with a different broadening associated with solvated $I_2$. We also notice that the shake-up features of $I_3^-$ at ∼59 eV and ∼61 eV are not modeled[47], but this point does not have any significant impact on the current analysis. Since the distortions influence the selection rules, the shake-up could contain additional information, which we unfortunately cannot address here due to spectral overlap of this feature and the direct photemission from Li 1s of the $Li^+$ counterion.

In the derived $I_3^-$ spectrum in red in panel b in Figure 8 (from Figure 6), the area ratios between the different peaks have been used to fix the relative amounts of $I_3^-$ and $I^-$. From the preparation of the aqueous solution, we would for stoichiometric reasons expect an $I^-/I_3^-$ ratio close to 1:1. However, we see evidence of dissociation of $I_3^-$ and therefore some additional $I^-$ may be present. To quantify the spectral response to the uncertainty in the concentrations, we subtracted the LiI contribution with varying weight from the spectrum containing both $LiI_3$ and LiI (four different $I^-/I_3^-$ ratios are shown).
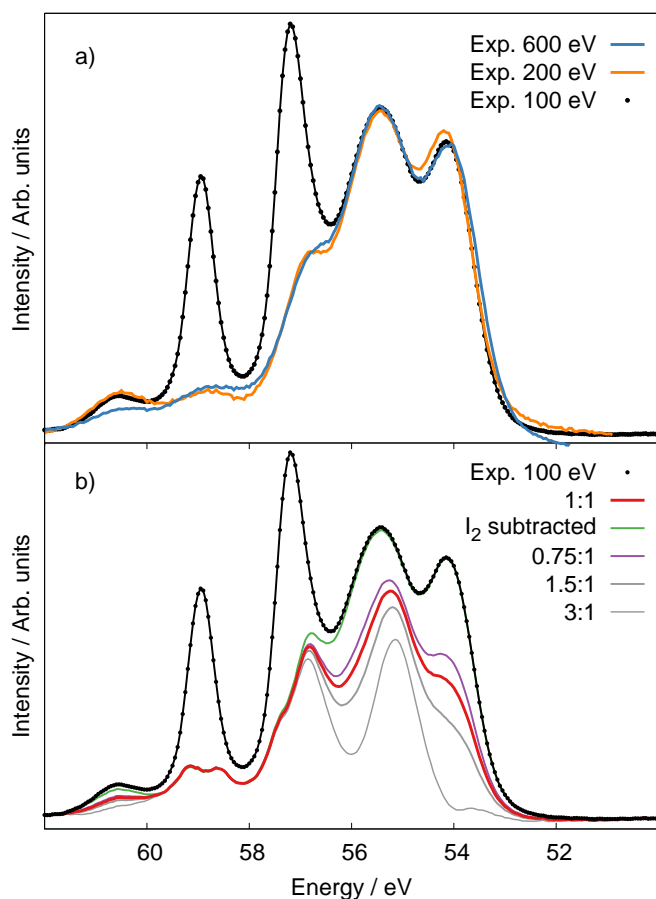
**Fig. 8** (a) Photoelectron I4d spectra of aqueous solution measured at BESSY II and MAX IV. (b) Spectra of $I_3^-$ (aq) resulting from different subtraction schemes, varying the weight of the subtracted LiI contribution from the MAX IV data containing both $LiI_3$ and LiI, are compared.

We see that even with large variations in the ratios, the low binding energy shoulder remains. To make the shoulder virtually disappear, we need to use an ion ratio of 3:1, which is unrealistic – given how the solution was prepared – since it would suggest that 3 times more $I^-$ is present than $I_3^-$. Due to the surface sensitivity in PE spectroscopy, surface enhancement of some solvated species with respect to the solute distribution in the bulk solution would be seen as an increased area of the corresponding PE peak. The penetration depth of the incident photon varies however with the energy; from the similarity of the data at different photon energies in panel a in Figure 8, we can therefore exclude strong variation with probing depth and the surface propensity of the ions as the reason for variation in the ion ratio. Hence, based on the spectra in Figure 8, we can conclude that the derived PE spectrum of $I_3^-$ (aq) in Figure 6, are indeed predominantly originating from $I_3^-$.

## 5 Conclusions

From other investigations, it is known that symmetry breaking fluctuations are important for the solvation of simple ions [48,49] as well as for determining pathways after photoexcitation in solution [50]. The asymmetry in the hydrated $I_3^-$ ion makes it suitable for studies of the coupling of collective H-bond dynamics and internal solute vibrations. Previous calculations showed evidence of symmetry breaking of the $I_3^-$ ion in aqueous solution, in contrast to polar solvents with no hydrogen bonds, in which $I_3^-$ remains linear and symmetric. [20–22]

In the present study we have studied the dynamics with ab initio molecular dynamics simulations and shown that the asymmetry can be identified in core-level PE spectroscopy. The structure of the aqueous $I_3^-$ ion were compared directly with recent EXAFS measurements [18]. The EXAFS results along with previous Raman measurements [17] and extensive theoretical investigations [20–22] strongly support our results. The insight into the electronic structure from our core-level measurements and from the ab initio MD simulations adds to the understanding of the solvation of the $I_3^-$ ion by showing how the electronic structure is effected by large geometrical distortions. Hydrogen bond interactions amplify the asymmetry of the ion and induce charge localization on the terminal iodine atom with the longest I–I bond to the center atom. For solvation in alcohols [17,18], it seems that the structure and motion of the $I_3^-$ ion, as detected in EXAFS and Raman are not sufficiently asymmetric to induce a charge localization, large enough to be noticeable in the I4d core-level spectra. We hope that the here presented results will stimulate further investigations with time-resolved IR spectroscopy of how the local H-bond exchange around an aqueous ion [51–53] propagates over the H-bond network into that of a neighboring ion. For solar cells, activation of the $I_3^-$ ion in asymmetric environments could be important for its function through interactions with surfaces and dye molecules. It also gives a mechanism for iodide polymerization [4]. Polymerization, induced by water impurities, could cause aging of the solar cells.

In conclusion, we have shown that the $I_3^-$ ion in the MD simulation of $LiI_3$(aq) undergoes large amplitude fluctuations in the asymmetric I–I stretch and that this asymmetry is strongly manifested in the I4d core-level PE spectrum. This transient (partial) dissociation of the $I_3^-$ ion in aqueous solution can be ascribed to its high polarizability as seen in charge redistribution; the simulation snapshot in Figure 3 illustrates clearly that the nearly detached iodine atom is well solvated by hydrogen bonding, since the greatest portion of the negative charge is localized on that site. The remaining neutral $I_2$ moiety is only weakly solvated. The study highlights the importance of using ab initio MD simulations in the study of highly polarizable ions in solution. Through ab initio spectrum calculations, signatures of collective dynamics in the hydrogen

bond network can be related to the solvent dependence in the experimental I4d core-level PE spectra. Consequently, we have presented a unique example in which PE spectroscopy provides evidence for solvent-induced changes in the solute geometry.

# 6 Acknowledgements

# References

1 B. O'Regan and M. Grätzel, *Nature*, 1991, **353**, 737–740.

2 G. Boschloo and A. Hagfeldt, *Acc. Chem. Res.*, 2009, **42**, 1819–1826.

3 S. Martiniani, A. Y. Anderson, C. Law, B. C. O'Regan and C. Barolo, *Chem. Commun.*, 2012, **48**, 2406–2408.

4 L. Kloo, J. Rosdahl and P. Svensson, *Eur. J. Inorg. Chem.*, 2002, **2002**, 1203–1209.

5 P. Svensson and L. Kloo, *Chem. Rev.*, 2003, **103**, 1649–1684.

6 T. Daeneke, Y. Uemura, N. W. Duffy, A. J. Mozer, N. Koumura, U. Bach and L. Spiccia, *Adv. Mater.*, 2012, **24**, 1222–1225.

7 C. Law, S. C. Pathirana, X. Li, A. Y. Anderson, P. R. F. Barnes, A. Listorti, T. H. Ghaddar and B. C. O'Regan, *Adv. Mater.*, 2010, **22**, 4505–4509.

8 Z. Yu, N. Vlachopoulos, M. Gorlov and L. Kloo, *Dalton Trans.*, 2011, **40**, 10289–10303.

9 A. Hagfeldt, G. Boschloo, L. Sun, L. Kloo and H. Pettersson, *Chem. Rev.*, 2010, **110**, 6595–6663.

10 S. M. Feldt, E. A. Gibson, E. Gabrielsson, L. Sun, G. Boschloo and A. Hagfeldt, *J. Am. Chem. Soc.*, 2010, **132**, 16714–16724.

11 J. Burschka, N. Pellet, S.-J. Moon, R. Humphry-Baker, P. Gao, M. K. Nazeeruddin and M. Graetzel, *Nature*, 2013, **499**, 316+.

12 M. M. Lee, J. Teuscher, T. Miyasaka, T. N. Murakami and H. J. Snaith, *Science*, 2012, **338**, 643–647.

13 C. Law, O. Moudam, S. Villarroya-Lidon and B. O'Regan, *J. Mater. Chem.*, 2012, **22**, 23387–23394.

14 E.-H. Kong, J. Lim, Y.-J. Chang, Y.-H. Yoon, T. Park and H. M. Jang, *Adv. Energy Mater.*, 2013.

15 C. Law, O. Moudam, S. Villarroya-Lidon and B. O'Regan, *J. Mater. Chem.*, 2012, **22**, 23387–23394.

16 W. Xiang, F. Huang, Y.-B. Cheng, U. Bach and L. Spiccia, *Energy Environ. Sci.*, 2013, **6**, 121–127.

17 A. E. Johnson and A. B. Myers, *J. Phys. Chem.*, 1996, **100**, 7778–7788.

18 K. H. Kim, J. H. Lee, J. Kim, S. Nozawa, T. Sato, A. Tomita, K. Ichiyanagi, H. Ki, J. Kim, S.-i. Adachi and H. Ihee, *Phys. Rev. Lett.*, 2013, **110**, 165505.

19 H. Sakane, T. Mitsui, H. Tanida and I. Watanabe, *J. Synchrotron Radiat.*, 2001, **8**, 674–676.

20 C. Margulis, D. Coker and R. Lynden-Bell, *J. Chem. Phys.*, 2001, **114**, 367–376.

21 C. Margulis, D. Coker and R. Lynden-Bell, *Chem. Phys. Lett.*, 2001, **341**, 557–560.

22 F. S. Zhang and R. M. Lynden-Bell, *Phys. Rev. Lett.*, 2003, **90**, 185505.

23 B. Winter, R. Weber, W. Widdra, M. Dittmar, M. Faubel and I. Hertel, *J. Phys. Chem. A*, 2004, **108**, 2625–2632.

24 B. Winter, *Nuclear Instruments and Methods in Physics Research Section A: Accelerators, Spectrometers, Detectors and Associated Equipment*, 2009, **601**, 139 – 150.

25 B. Winter and M. Faubel, *Chem. Rev.*, 2006, **106**, 1176–1211.

26 N. Ottosson, K. J. Børve, D. Spångberg, H. Bergersen, L. J. Sæthre, M. Faubel, W. Pokapanich, G. Öhrwall, O. Björneholm and B. Winter, *J. Am. Chem. Soc.*, 2011, **133**, 3120–3130.

27 H. Bergersen, R. R. T. Marinho, W. Pokapanich, A. Lindblad, O. Björneholm, L. J. Saethre and G. Öhrwall, *J Phys.-Condens. Mat.*, 2007, **19**, 326101.

28 R. Car and M. Parrinello, *Phys. Rev. Lett.*, 1985, **55**, 2471–2474.

29 CPMD, http://www.cpmd.org/, Copyright IBM Corp 1990-2008, Copyright MPI für Festkörperforschung Stuttgart 1997-2001.

30 S. K. Eriksson, I. Josefsson, N. Ottosson, G. Öhrwall, O. Björneholm, A. Hagfeldt, M. Odelius and H. Rensmo, *Unpub.*, 2013, XX.

31 A. D. Becke, *Phys. Rev. A*, 1988, **38**, 3098–3100.

32 C. Lee, W. Yang and R. G. Parr, *Phys. Rev. B*, 1988, **37**, 785–789.

33 S. Grimme, *J. Comp. Chem.*, 2006, **27**, 1787–1799.

34 N. Troullier and J. L. Martins, *Phys. Rev. B*, 1991, **43**, 1993–2006.

35 L. Kleinman and D. M. Bylander, *Phys. Rev. Lett.*, 1982, **48**, 1425–1428.

36 S. Goedecker, M. Teter and J. Hutter, *Phys. Rev. B*, 1996, **54**, 1703–1710.

37 C. Hartwigsen, S. Goedecker and J. Hutter, *Phys. Rev. B*, 1998, **58**, 3641–3662.

38 B. O. Roos, P. R. Taylor and P. E. M. Siegbahn, *Chem. Phys.*, 1980, **48**, 157–173.

39 F. Aquilante, L. De Vico, N. Ferré, G. Ghigo, P.-Å. Malmqvist, P. Neogrády, T. B. Pedersen, M. Pitonak, M. Reiher, B. O. Roos, L. Serrano-Andrés, V. Veryazov and R. Lindh, *J. Comp. Chem.*, 2010, **31**, 224–247.

40 N. Douglas and N. M. Kroll, *Ann. Phys.*, 1974, **82**, 89–155.

41 B. Hess, *Phys. Rev. A*, 1986, **33**, 3742–3748.

42 B. O. Roos, R. Lindh, P.-Å. Malmqvist, V. Veryazov and P.-O. Widmark, *J. Phys. Chem. A*, 2004, **108**, 2851–2858.

43 P.-Å. Malmqvist, B. O. Roos and B. Schimmelpfennig, *Chem. Phys. Lett.*, 2002, **357**, 230–240.

44 L. Gagliardi, R. Lindh and G. Karlström, *J. Chem. Phys.*, 2004, **121**, 4494.

45 T. Penfold, I. Tavernelli, M. Doemer, R. Abela, U. Röthlisberger and M. Chergui, *Chem. Phys.*, 2013, **410**, 25 – 30.

46 H. Sato, F. Hirata and A. B. Myers, *J. Phys. Chem. A*, 1998, **102**, 2065–2071.

47 M. Arbman, S. Holmberg, M. Lundholm, H. Siegbahn, O. Gropen and U. Wahlgren, *Chem. Phys.*, 1983, **81**, 113–119.

48 J. Thøgersen, J. Rehault, M. Odelius, T. Ogden, N. K. Jena, S. J. Knak-Jensen, S. R. Keiding and J. Helbing, *J. Phys. Chem. B*, 2013, **117**, 3376–3388.

49 D. Y.Vorobyev, C.-H.Kuo, D. G. Kuroda, J. N. Scott, J. M. Vanderkooi and R. M. Hochstrasser, *J. Phys. Chem. B*, 2010, **114**, 2944–2953.

50 W. Zhang, M. Ji, Z. Sun and K. J. Gaffney, *J. Am. Chem. Soc.*, 2012, **134**, 2581–2588.

51 M. Ji, M. Odelius and K. J. Gaffney, *Science*, 2010, **328**, 1003–1005.

52 C.-H. Kuo, D. Y. Vorobyev, J. Chen and R. M. Hochstrasser, *J. Phys. Chem. B*, 2007, **111**, 14028–14033.

53 J. Borek, F. Perakis, F. Kläsi, S. Garrett-Roe and P. Hamm, *J. Chem.*

*Phys.*, 2012, **136**, 224503.